Chemical Engineering Science 253 (2022) 117548

Contents lists available at ScienceDirect

Chemical Engineering Science

journal homepage: www.elsevier.com/locate/ces

Application of machine learning in colloids transport in porous media studies: Lattice Boltzmann simulation results as training data

H. Aslannejad [a,*], M. Samari-Kermani [a], H. Mohammad Nezami [b], S. Jafari [c], A. Raoof [a]

[a] Department of Earth Sciences, Utrecht University, Utrecht, the Netherlands
[b] Hydrogen and Fuel Cell Research Lab., Chemical Engineering Department, Faculty of Engineering, University of Kashan, Iran
[c] Mechanical Engineering Department, Shahid Bahonar University of Kerman, Kerman, Iran

HIGHLIGHTS

- Four main parameters affecting the clogging process in a porous material were chosen; ionic strength, velocity, zeta potential, and particle diameter.
- Using Lattice Boltzmann simulations, it is possible to study the particles transfer through pores and throats. However, it is computationally very expensive.
- A limited number of Lattice Boltzmann simulations were performed and then the results were used as feed to machine training.
- The training process yielded a well-trained code which is able to predict the clogging condition in a matter of few seconds.

ARTICLE INFO

Article history:
Received 21 October 2021
Received in revised form 24 December 2021
Accepted 18 February 2022
Available online 24 February 2022

Keywords:
Colloid transport
Artificial neural network
Clogging
Hydrodynamic effect
Colloid size effect
Lattice Boltzmann method
Stochastic modeling
Deep learning
Machine learning

ABSTRACT

Colloid transport through a porous medium changes geometrical and hydraulic properties of the pore space. The impact of this effect depends on the colloid types and pore space surface properties which determine the likelihood of pore clogging. Colloid attachment and subsequent detachment are key factors in pore clogging. In this study, the impact of four major fluid and colloids properties on the pore surface and hydraulic conductivity alteration during colloids transport were evaluated using machine learning. These four parameters include solution ionic strength, zeta potential, colloid size and fluid flow velocity.

A combined lattice Boltzmann-smoothed profile method was used to simulate accurately coupled mechanisms governing colloid transport to evaluate the impact of the four parameters on the resulting pore space properties after colloid transport. The result of several simulations revealed significant changes of pore surface coverage by the attached colloids, and conductivity, void fraction and coordination number of colloid agglomerates created during transport of individual colloids. Since the simulation of the impact of combination of all possible sets of four parameters is very time consuming, an Artificial Neural Network (ANN) was used as a prognostic method to use the results of several simulations to predict the behavior for a wide range of pore, colloidal and fluid properties. Reported results from a set of 162 simulation case studies for different possible combination of solution ionic strength, zeta potentials, colloid size and flow velocity were selected as input parameters for the machine learning. Four output parameters, namely, pore surface coverage, conductivity, void fraction and coordination number of the colloidal particles were selected.

To lower the prediction error value, which is targeted to be lower than 10%, networks were trained 50 times using a MATLAB code, and in each training, after at most 10 epochs, networks were trained. A maximum relative error value of 8.95% was obtained, which is very well within the range of training quality criteria. The results show that the ANN can profoundly predict the simulation outcomes for a wide range of ionic strength (*IS*) and can be directly used to obtain the value of dependent variables through simple calculations using network weights and transfer functions.

1. Introduction

Along with the liquid and gas phases moving through pores of a porous medium solid particles can become mobile and transfer

* Corresponding author at: Environmental Hydrogeology Group, Department of Earth Sciences, Universiteit Utrecht, Princetonplein 9, 3584 CC Utrecht, the Netherlands.
E-mail address: H.aslannejad@uu.nl (H. Aslannejad).

https://doi.org/10.1016/j.ces.2022.117548
0009-2509/

together with the flowing fluid. A well-known example of solid particle transport in porous media is the spread of contamination in soil. This constitutes a major branch of solid particle transport in porous media.

Colloids are defined as small, suspended particles in a size range of 1 nm to 10 μm and can belong to a wide range of materials such as ink pigments, latex particles, viruses, fine soil grains etc. Transport of these fine particles is important as they play an important role in water management, geoscience studies, industrial processes as well as medical sciences.

Several physical processes have influence on colloids transport and separation. While they move through the pores of a porous medium, depending on their size, their energy interaction with solid surface of pores and throats, and retention at low velocity regions.

Several researchers tried to study deeply the interaction of colloids and solid/water interface to reveal the parameters affecting colloid deposition on the surface and clogging of the pores. Bradford et al. (Bradford et al., 2007; Bradford et al., 2006) studied the colloid-solid interaction in saturated condition. They explored the coupled physical and chemical mechanisms of colloid straining under unfavorable conditions. To represent colloids, they used negatively charged Latex particles (1.1 – 3 μm) and sand grains (150 – 360 μm). For fluid, they used solutions with ionic strength of 6 – 106 mM and flow velocity of 0.1 – 0.45 cm min^{-1}. They found that by increasing the ionic strength, lowering flow rate and increasing the colloid to grain size ration, deposition of colloid, as expected, rises. In another work, Torkzaban et al. (Torkzaban et al., 2008) conducted experimental and computational simulations to study the influence of water saturation, ionic strength and grain size on transport of Latex particles (diameter of about 1 μm) in packed column type porous media. They used negatively charged hydrophilic colloids in a solution with a pH value of 10. Their experiments and modeling showed that the colloids retention was mainly found under low velocity regimes in saturated and unsaturated conditions. The retention was enhanced by lower water content.

In industrial applications, the ink suspension used in pigmented inkjet printers has ink pigments and latex particles inside. While the ink pigments are a few nanometers in diameter the latex particles are much larger and are about 100 nm. The printing paper can be both coated or uncoated. In both cases, all comprising layers are porous; in case of coated paper, the size of pores starts from 20 nm up to 25 μm, while uncoated paper has larger pores from 1 to 25 μm (Aslannejad and Hassanizadeh, 2017; Aslannejad et al., 2019; Aslannejad et al., 2017).

Buckley (Buckley, 2012) studied the creation and deposition of asphaltene during oil transport. A long stainless-steel tube was used as a capillary tube to investigate the separation of asphaltene flocs from unstable oil. The results of such an experiment yielded deposition rate of asphaltene under wellbore conditions. A. Lawal et al. (Lawal et al., 2011) also performed a similar study to investigate the permeability change of a porous media during asphaltene deposition process. They developed a dynamic-filtration model. S. Boek et al. (Boek et al., 2008; Boek et al., 2010; Li et al., 2017) conducted a fundamental study on the aggregation and deposition of colloidal asphaltene in reservoir rock. They used a stochastic rotation dynamic (SRD) to perform the simulations. In addition to that, they conducted experiments using glass capillary tubes to monitor the dynamics of asphaltene precipitation and deposition. By combination of the simulation and experiments, they could find out the flow conditions associated with the asphaltene deposition process.

Kermani et al. (Samari Kermani et al., 2020; Samari-Kermani et al., 2021) used a lattice Boltzmann- smoothed profile method to explore the coupled effects of ionic strength, zeta potential, colloid size and flow velocity on transport and retention of colloids in porous media. The interactions among moving and attached particles were considered under both favorable and unfavorable conditions. Their results showed an increase in aggregates connectivity and surface coverage, but a decrease in pore void fraction and conductivity as pore velocity decreased. In addition, a raise in ionic strength caused a decrease in pore void fraction and conductivity and an increase in colloids connectivity.

There are different simulation methods, like the one mentioned above by Kermani et al., to obtain the fluid and colloid flow in porous media and study the pore properties after colloid passage. However, they are tending to take longer time or even fail in complex cases. On the other hand, deep learning methods have been introduced as a tool to use experimental results or those obtained from simulations as training material and then to predict variables of interest. The technique is based on training layers of a convolutional neural network in order to find relationships among various input and output data. Deep learning methods usually need a benchmark dataset since they need a large amount of data and their training quality should be evaluated quantitively. Application of deep learning methods in fluid flow in porous media studies has gained a great interest in recent years. Wu et al. (Wu et al., 2018) introduced a framework to obtain permeability values out of imaged porous media. They generated different porous media geometries and run fluid dynamics simulation to calculate their permeabilities. Then the simulation results were used to train a convolutional neural network to predict permeability values for a new and unique pores medium geometry without any need to run the fluid dynamics simulation. They concluded that by doing so, the computational time was reduced by several orders of magnitude. Sudakov et al. (Sudakov et al., 2018) conducted a similar study but by using pore network modeling as the simulation tool to obtain permeability values. Digitized rock samples imaged using X-ray microtomography were used as porous media. 3D images and 2D slices were used as an input feature for the predictive model. The pore network approach indeed used a simplified version of the pore network to facilitate the fluid flow simulation. Their results demonstrated the applicability of machine learning tools to obtain the permeability of the media by using their tomography images.

In a recent work, Kamrava et al. (Kamrava et al., 2020) studied the relation between morphology of a porous medium and its permeability. They developed a new network which uses deep learning as a tool to link the permeability of the porous medium to its morphology. Their network is a hybrid of a traditional artificial neural network and deep learning algorithm. The input of their model included 3D images of the medium, synthetic unconsolidated porous media generated by a Boolean method and stochastic realizations generated by image analysis and reconstruction. Their trained network was able to predict accurately the permeability value for a variety of porous media. Santos et al. (Santos et al., 2020) moved one step further and used the 3D morphology of the porous medium and generalized single phase flow of a fluid through the material. They showed that a 3D convolutional neural network is able to find a relationship between morphological features and the steady state solution of Navier-Stokes equation in laminar condition. Their trained model was able to extract spatial relations between fluid flow and pore network characteristics of the medium. They used four main geometric features of the porous medium, namely, Euclidean distance, maximum inscribed sphere, time of flight from left to right and from right to left. The second category of input data to train the code was single phase fluid flow simulation in the domain. The trained model was able to obtain sufficient and accurate information about fluid flow in pores of the domain in less than a second, which is several magnitudes faster than performing time-expensive numerical simulations. In addition to that, even so the trained code used a simple synthetic

geometry to be trained, the model was able to predict properly the results for real samples like granular rocks and carbonates. In a similar approach, Kamrava et al. (Kamrava et al., 2021) developed and trained a machine learning method that takes the morphology of a porous medium and predicts its flow properties such as pressure and velocity in pores of the medium. They evaluated the performance of the model on 200 membrane samples and porous media. The results showed a very good agreement with direct numerical simulation.

Another application of the machine learning approaches is to predict the performance of a porous layer such as during nanofiltration. Hu et al. (Hu et al., 2021) developed such a predictive models using artificial intelligence algorithms. They carried out a principal component analysis to find out the most important parameters affecting the permeance and rejection of the medium. They trained three artificial intelligence models, namely artificial neural network, support vector machine and random forest. With the trained models they were able to predict the permeance and rejection with accuracy of 91 and 98%, respectively. They claimed that the trained model is not only able to predict the performance of a made filter but also can be used to design better membranes.

In this paper, we propose a novel approach based on using an artificial neural network to predict the pore properties after passage of a colloid. As set of previously performed Lattice Boltzmann simulations were used as input parameters to train the model. A set of four main parameters affecting the colloid transport in the pore media were selected; solution ionic strength, zeta potentials, colloid size and flow velocity. The four input parameters were chosen to provide a wide range which covers both the clogging and not-clogging condition of the pore/throats. The results of the Lattice - Boltzmann simulations were also divided into four main parameters defining pore properties after colloid/fluid passage. The output parameters are: pore surface coverage with attached colloids, conductivity of the pore, void fraction and coordination number of the colloid. After the training process, the trained model was able to predict the set of four output parameters without any need to run Lattice – Boltzmann simulations for a new case consisting of a unique set of four input parameters. In other words, the trained model was able to predict the pore properties, after colloid transport, in less than a second.

2. Methodology

2.1. Direct pore scale numerical simulation

In this paper, the generated results of Samari-Kermani were used to train the artificial neural network. Here a brief explanation of the numerical simulation is presented. More details can be found in (Samari Kermani et al., 2020; Samari-Kermani et al., 2021).

2.2. Geometry

The geometry is a single sinusoidal pore-throat to provide converging–diverging streamlines to represent the pore structure and the flow in porous media. A 400 × 100 rectangular grid is used to define the domain. The pore is 200 μm long, and 50 μm wide at the inlet and the outlet which reduces to 20 μm at the throat, Fig. 1.

2.3. Fluid flow simulation and boundary conditions

The fluid flow is laminar and simulated using a D2Q9 (two-dimensional lattice with nine directional flow vectors, eight representing the radial flow and one the null flow state) lattice Boltzmann model with BGK (Bhatnagar-Gross-Krook (BGK) collision) approximation and an external force term (Lattice Boltzmann Method And Its Application In Engineering - Zhaoli Guo, 2021; Krüger et al., 2017). Equation (1) shows the discretized form of Boltzmann equation that considers fluid particles as distribution functions (f_α) which stream along lattice links in α directions and collide at lattice nodes ($\boldsymbol{x}$) to relax toward their equilibrium values (f_α^{eq}). In this equation, c, t ,τ, $\boldsymbol{F}$, and

$$\boldsymbol{e}_\alpha = \begin{cases} (0,0) & \alpha = 0 \\ (1,0),(0,1),(-1,0),(0,-1) & \alpha = 1,2,3,4 \\ (1,1),(-1,1),(-1,-1),(1,-1) & \alpha = 5,6,7,8 \end{cases}$$

are lattice speed, time, dimensionless relaxation time , external body force and the discrete velocity vectors in the nine α directions of the D2Q9 model, respectively.

$$f_\alpha(\boldsymbol{x}+\boldsymbol{e_\alpha}\Delta t, t+\Delta t) - f_\alpha(\boldsymbol{x},t) = -\frac{1}{\tau}\left[f_\alpha(\boldsymbol{x},t) - f_\alpha^{eq}(\boldsymbol{x},t)\right] + 3\omega_\alpha \rho \boldsymbol{e}_\alpha.\boldsymbol{F}/c^2 \quad (1)$$

The equilibrium distribution function in each direction is calculated by Equation (2):

$$f_\alpha^{eq} = \omega_\alpha \rho\left[1 + 3\frac{\boldsymbol{e_\alpha}.\boldsymbol{u}}{c^2} + \frac{9}{2}\frac{(\boldsymbol{e_\alpha}.\boldsymbol{u})^2}{c^4} - \frac{3}{2}\frac{\boldsymbol{u}.\boldsymbol{u}}{c^2}\right] \quad (2)$$

where $\omega_\alpha = \begin{cases} 4/9 & \alpha = 0 \\ 1/9 & \alpha = 1,2,3,4 \\ 1/36 & \alpha = 5,6,7,8 \end{cases}$

shows the weight coefficients. At each time step, distribution functions are used to calculate macroscopic properties such as fluid density, $\rho(\boldsymbol{x},t) = \sum_{\alpha=0}^{8} f_\alpha(\boldsymbol{x},t)$, and velocity, $\boldsymbol{u}(\boldsymbol{x},t) = \frac{1}{\rho(\boldsymbol{x},t)}\sum_{\alpha=0}^{8}\boldsymbol{e_\alpha} f_\alpha(\boldsymbol{x},t)$.

Constant velocity inlet, constant pressure outlet (Zou and He, 1997), and no slip boundary conditions are implemented at the inlet, outlet, and the curved pore-throat surfaces (Bouzidi et al., 2001), respectively.

Solid particles simulation and the coupling between fluid and solid phases:

Solid particles are simulated using the smoothed profile method [SPM] which defines the fluid and solid domains at position × and time t through a $\varphi(\boldsymbol{x},t) = \sum_{P=1}^{N_P}\varphi_P(\boldsymbol{x},t)$ function (Jafari et al., 2011). Each of the N_P particles inside the domain are represented by $\varphi_P(\boldsymbol{x},t)$ as shown in Equation (3). This function takes the value of zero inside the fluid phase, takes the value of one inside the solid particles, and smoothly changes from zero to one in the interface thickness,ξ. In Equation (3), R_P, and $\boldsymbol{R}_P$ are each particle's radius and center position, respectively.

$$\varphi_P(\boldsymbol{x},t) = s(R_P - |\boldsymbol{x} - \boldsymbol{R}_P(t)|) \quad (3)$$

$$s(L_P) = \begin{cases} 0 & L_P < -\xi/2 \\ \frac{1}{2}(sin(\frac{\pi L_P}{\xi}) + 1) & |L_P| \le \xi/2 \\ 1 & L_P > \xi/2 \end{cases}$$

The particles' velocity field, $\boldsymbol{u_P}(\boldsymbol{x},t)$, is calculated by Equation (4) where $\boldsymbol{U}_{C_p}$, and $\boldsymbol{\omega}_P$ are the respective translational and angular velocity of each particle.

$$\varphi(\boldsymbol{x},t)\,\boldsymbol{u_P}(\boldsymbol{x},t) = \sum_{P=1}^{N_p}\varphi_p(\boldsymbol{x},t)\left[\boldsymbol{U}_{C_p}(t) + \boldsymbol{\omega}_P \times \{\boldsymbol{x} - \boldsymbol{R}_P(t)\}\right] \quad (4)$$

When the velocity field is known, hydrodynamic forces (F_P^H) and torques (T_P^H) implemented on each particle from the fluid can be obtained using Equations (5) and (6). In these equations, ρ shows the density of each particle, and it is considered to account for the mass of each particle.

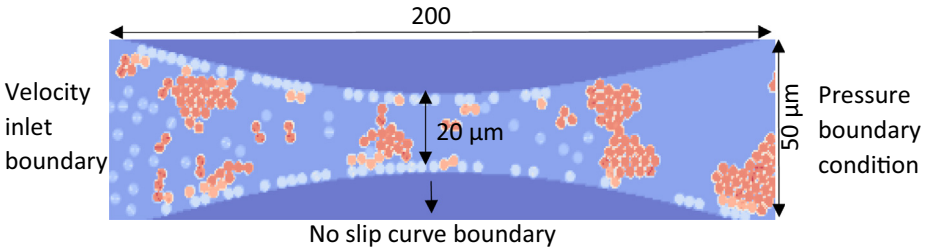

Fig. 1. Pore-throat geometry and boundary conditions.

$$F_P^H = \int_{\forall_p} \rho\varphi(\boldsymbol{x},t)(\boldsymbol{u}(\boldsymbol{x},t) - \boldsymbol{u}_p(\boldsymbol{x},t))\, d\forall_p \tag{5}$$

$$T_P^H = \int_{\forall_p} (\boldsymbol{x} - \boldsymbol{R}_P) \times \rho\varphi(\boldsymbol{x},t)(\boldsymbol{u}(\boldsymbol{x},t) - \boldsymbol{u}_p(\boldsymbol{x},t))\, d\forall_p \tag{6}$$

In SPM, the body force $f_H(\boldsymbol{x},t) = -\varphi(\boldsymbol{x},t)(\boldsymbol{u_P}(\boldsymbol{x},t) - \boldsymbol{u}(\boldsymbol{x},t))$, resulting from the fluid–solid interactions, is inserted on each fluid node covered by a solid particle. This force is then replaced by the external force $\boldsymbol{F}$ in Equation (1) to account for the coupling between fluid flow and particles transport. This way, not only the effect of fluid flow on particles transport, but also the effect of particles on changing the flow streamlines is considered. More detailed information about SPM and its implementation to study particles transport can be found in (Samari Kermani et al., 2020; Samari-Kermani et al., 2021).

2.4. Particle's transport and behavior

To simulate particle transport, the Lagrangian method is selected to track each particle's motion. In addition to drag and lift forces (F^H) calculated by SPM, gravitational and buoyancy forces (F^G), DLVO (Derjaguin-Landau-Verwey-Overbeek) interactions among particles ($\boldsymbol{F}_{P-P}^{DLVO}$), and DLVO interactions between particles and the pore surface ($\boldsymbol{F}_{P-P}^{DLVO}$) are considered as well (Derjaguin and Landau, 1993; Verwey, 1947). Knowing all the forces and torques (T_p), new translational and angular velocities of each particle ($\boldsymbol{U}_{C_p}, \boldsymbol{\omega}_p$) together with its new position ($\boldsymbol{R}_P$) are obtained using Equations 7–9. In these equations, M_P and I_P are each particle's mass and moment of inertia, respectively. The detailed information of each force can be found in (Samari Kermani et al., 2020; Samari-Kermani et al., 2021)

$$M_P \frac{d\boldsymbol{U}_{C_P}}{dt} = \boldsymbol{F}_P^H + \boldsymbol{F}_P^G + \boldsymbol{F}_{P-P}^{DLVO} + \boldsymbol{F}_{P-S}^{DLVO} \tag{7}$$

$$I_P.\dot{\boldsymbol{\omega}}_P = \boldsymbol{T}_P \tag{8}$$

$$\frac{d\boldsymbol{R_P}}{dt} = \boldsymbol{U}_{C_P} \tag{9}$$

Initially, there is no particle inside the pore, and the flow is simulated to reach the steady state. While the flow is steady, particles start to enter the pore at random heights. To be able to compare the results, the particles injection rate for all particle sizes and flow velocities is equal to 1188 μm^2 of particle surface per injected solution pore volume (PV). For example, this value is equal to the injection rate of 15 particles of 10 μm per PV.

Four parameters, each with three different values are selected to study particle behavior under various conditions. These parameters include particles diameter (dp = 3, 5, 10 μm), solution ionic strength (IS = 0.001, 0.05, 0.3 M), pore zeta potential ($\zeta_S = \pm 17.5, \pm 45.56, \pm 60$mV) and chosen particle zeta potential ($\zeta_P = -17.5, -45.56, -60$ mV), and mean flow velocity (U = 1, 5, 10 m/day). In all the simulations, the flow is aminar, the fluid is water with density of 1000 $\frac{kg}{m^3}$ and the density of particles is 1055 $\frac{kg}{m^3}$. Combination of these parameters results in 81 simulations for favorable deposition conditions ($\frac{\zeta_P}{\zeta_S} = -1$), and 81 simulations for unfavorable deposition conditions ($\frac{\zeta_P}{\zeta_S} = 1$).

It is worth mentioning that under favorable conditions, deposition of particles on the pore surfaces assumed to be irreversible and at the primary distance of the surface. However, under unfavorable conditions, deposition is assumed to be reversible and at the secondary minimum. Based on the forces and torques inserted on each particle at each time step, the particle can remain immobile at the point of secondary minimum, and so can attach tightly to the surface, can roll over the surface toward the outlet, or can detach from the surface to join the bulk flow (Samari Kermani et al., 2020; Samari-Kermani et al., 2021). Additionally, in these simulations, the suspension is not diluted; meaning that the particles can have secondary minimum interactions with each other to make agglomerates which can significantly affect particles transport and behavior.

2.5. Parameters studied in this paper

In this paper, average coordination number of particles is selected to indicate aggregation possibility. This parameter shows the average number of particles connected to each individual particle through secondary minimum interactions.

Dimensionless pore hydraulic conductivity shows how easy the flow can move through the pore while single and aggregated particles are available in comparison with the initial situation when there is no particle inside the domain.

Dimensionless surface coverage shows the fraction of the upper and lower pore surfaces that are covered by deposited particles. The covered area is calculated by projecting the particles diameter on the sinusoidal surfaces.

Void fraction is a dimensionless parameter to show what fraction of the pore space is occupied by deposited particles in comparison with its initial value when there is no particle inside the pore. To calculate this parameter, deposited particles are not only the ones that are directly attached on the surface, but also the ones that are connected to the surface through their neighboring particles in an agglomerate.

The present study uses the time-averaged values of the above parameters obtained after injecting several pore volumes of the suspension. In the cases with clogging condition, the reported values are the ones related to the clogging time, when the dimensionless hydraulic conductivity reduces to nearly zero. Samples of the graphs showing the time dependency of these parameters are available in (Samari Kermani et al., 2020), and the obtained time-averaged values can be found in (Samari-Kermani et al., 2021).

2.6. Artificial neural network

Artificial Neural Network (ANN) is one of the well-known predictive methods used to find a solution when other statistical methods are not applicable. The advantages of this tool are the ability to learn from example datasets, fault tolerance, operation in a real-time environment, and forecasting non-linear data; all of them make this tool a widely used statistical approach. Moreover, ANN accurately fits in the nonlinear variable, which is an advantage compared to multivariate linear analysis based on linear variables (Stangierski et al., 2019).

An ANN is a functional imitation of the natural biological neurons, each of which is its fundamental data processing element. Like the biological neurons in the brain, it is made of simple but highly interconnected processors, also called neurons. Fundamentally, a biological neuron takes inputs from different sources, puts them together, performs a nonlinear operation on the input data and calculates the result. Weighted links are the source of neurons connections and signals are passed from one neuron to another by these connections. A number of input signals are received by each neuron through its connections and transmitted through outgoing neuron connections as output. The strength of each neuron input is demonstrated by the weights and its adjustment recurrently, leads to the neural network learning process (Urang et al., 2020).

In the feed-forward multi-layer neural network considered in this paper (Fig. 2), the neurons are arranged in several layers: an input layer containing one neuron for each independent variable and taking the input data, one or more hidden layers where the data are processed, and an output layer, containing one neuron for each dependent variable producing a result.

Each neuron connects with every neuron in the next layer. However, there are no connections among neurons in the same layer. The ANN learning process is based on adjusting weighted connections between neurons until the most efficient solution of a problem has been obtained. Moreover, providing both an input and output in the network allows for calculation of an error based on its target output and present output. This can be used for corrections of the network by updating its weights and to achieve optimal results (Stangierski et al., 2019).

2.7. Network design

The ANN was trained with a single hidden layer, and the transfer function for the hidden layer was tangent sigmoid, while for the output layer it was a pure linear function. The back propagation algorithm was used, which has proven successful in a wide range of applications (Carvalho et al., 2013). Ten neurons in the hidden layer were found to be enough after preliminary training and testing the ANN.

To compare the prediction ability of trained ANN two criteria of Mean Square Error (*MSE*) and correlation coefficient (*R*) were applied which are defined as flow:

$$MSE = \left[\sum_{1}^{N} (Q_{sim} - Q_{ANN})^2 / N\right] \tag{10}$$

$$R = \frac{\sum_1^N \left(Q_{sim} - \bar{Q}_{sim}\right)\left(Q_{ANN} - \bar{Q}_{ANN}\right)}{\sqrt{\left[\sum_1^N \left(Q_{sim} - \bar{Q}_{sim}\right)^2 \left(Q_{ANN} - \bar{Q}_{ANN}\right)^2\right]}} \tag{11}$$

where N is number of samples, Q_{sim} is Boltzmann simulation data and Q_{ANN} is ANN output. Furthermore, absolute value of relative error $E = \frac{Q_{sim} - Q_{ANN}}{Q_{sim}} \times 100$ was used to find the most error produced during each training. In this study four independent variables i.e., *IS*, *U*, *Z*, *D* and four dependent variables were considered i.e., *CN*, *COV*, *COND*, and *VOID*.

Performing multi-input multi-output training showed that the network would not yield a high *R* and a low *E* value and these

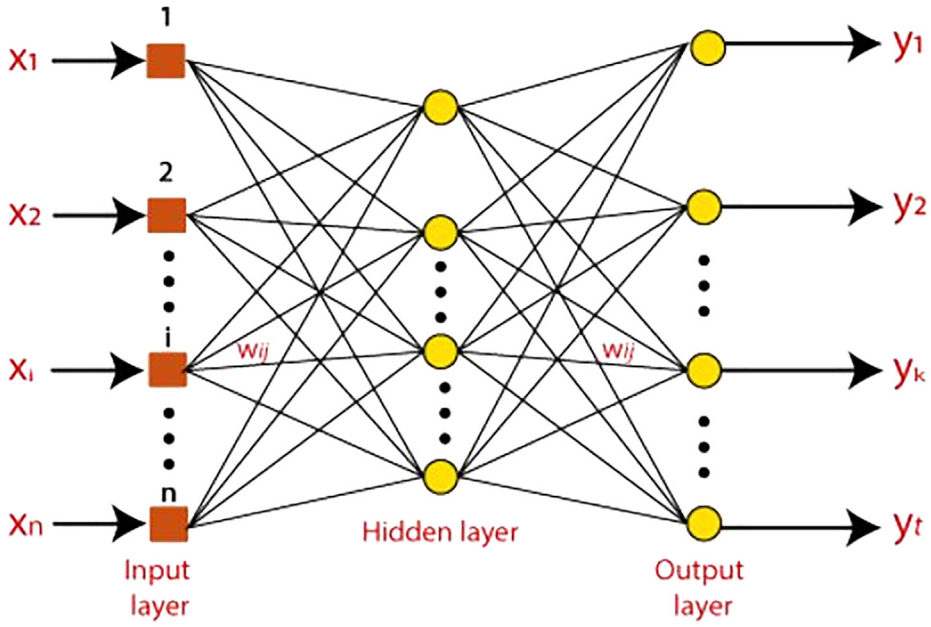

Fig. 2. A schematic diagram of a perceptron network (x_i is input, y_i is output. W_{ij} is weight. Yellow circles are transfer functions for hidden and output layers. Red squares are input transfer functions) (Artificial Neural Network Tutorial - Javatpoint n.d.). (For interpretation of the references to colour in this figure legend, the reader is referred to the web version of this article.)

Table 1
Training parameters of network for favorable condition.

	Aggregate coordination number	Surface coverage	Conductance	Void fraction
Low ionic strength: *IS* = 0.003				
R	0.9996	0.9994	0.9997	0.9985
MSE	3.2918×10^{-5}	2.4293×10^{-6}	6.8408×10^{-5}	1.5610×10^{-6}
E	5.44	7.40	5.76	0.3043
Medium ionic strength: *IS* = 0.05				
R	0.9995	0.9994	0.9996	0.9987
MSE	4.4687×10^{-4}	5.0351×10^{-5}	2.3114×10^{-5}	2.0265×10^{-5}
E	4.14	8.95	6.4340	1.98
High ionic strength: *IS* = 0.3				
R	0.9994	0.9999	0.9987	0.9998
MSE	3.4145×10^{-4}	2.9892×10^{-7}	9.6165×10^{-7}	5.1533×10^{-7}
E	6.71	5.21	5.3427	0.4179

results indicated that training was sufficient to correlate inputs and output data. Therefore, we transformed the network architecture to a multi-input and single-output form. This strategy helped to improve the input–output correlation but still prediction quality remained poor. Through examining each individual independent variable, we found that IS had a strong nonlinear relationship with outputs, and, therefore, had strong impact on preventing the ANN from reaching the learning goal. As a solution, the *IS*, as an independent variable, was categorized into 3 levels namely Low-IS = 0.003, Medium-IS = 0.05, High-IS = 0.3. Via this modification of the network, each output variable must divide according to *IS* subsections and hence 12 networks needed to describe all input output relationships and fittings (four dependent variables times three *IS* subsections). With this classification of *IS*, the learning process improved and the parameters *R* and *MSE* reached desired values as well.

For each dependent variable, 162 samples were available which came from Boltzmann simulations. After initial trainings and observing the results, it was found that 90%, 5% and 5% were suitable fractions for training, validation and test, respectively. MATLAB software was used for performing network training and due to short time required for training, Levenberg-Marquardt optimization algorithm was selected for network training.

3. Results and discussion

For each *IS* level, the parameters *R*, *MSE* and *E* are presented in Tables 1 and 2. To reach to a desired *E* value (to be less than 10%), networks were trained by a MATLAB routine and in each training after at most 10 epochs networks were trained.

3.1. Favorable condition

As given in Table 1, maximum relative error of 8.95% was obtained for favorable condition dataset, which fulfilled the training goal. Correlation coefficients (*R*) of all ANNs were above 0.995 and this value for *R* ensured that network outputs would be close enough to simulation data in the range of input and output data. Regression plots are presented in appendix A for the ANN trained in this step.

The results showed that the ANN can profoundly predict the simulation data in a wide range of *IS*. In other words, the trained model can be used directly to find the value of dependents values by simple calculations through network weights and transfer functions.

3.2. Unfavorable condition

MATLAB code also was used to find the neural network correlations for attachment under unfavorable condition. A maximum relative error of 9.3%, as given in Table 2, was calculated during the training phase, which is very well in the range of accepted training criteria. similar to the situation for training under favorable conditions, correlation coefficients (*R*) of all ANNs were calculated and were above 0.995, which means network outputs are sufficiently close to simulation data in the range of input and output data. In a\Appendix B, regression plots of the unfavorable condition training phase are illustrated. The obtained results clearly show that ANN is able to satisfactorily predict the simulation results under unfavorable adsorption condition.

4. Conclusion

A large amount of data from a previous work on direct numerical modeling of colloid adsorption was used to study the impact of colloids transport on geometrical and hydraulic properties of pore structures. A constricted pore-throat geometry consisting of two pores with a throat (which mimics the convergence and divergence character of the flow field) was chosen together with a range of conditions for the flowing fluid and colloids to simulate adsorptive colloid transport. As training feed, we have used results from 162 simulation cases (which were previously published by Samari-Kermani (Samari Kermani et al., 2020), in which a combined lattice Boltzmann-smoothed profile method was employed to study different possible conditions using for input parameters namely solution ionic strength, zeta potential, colloid size and flow velocity. The reported simulation results included hydrodynamic, gravity, buoyancy, van der Waals and electrostatic forces to simulate their impact on colloid transport and aggregation. The result of simulations was interpreted to provide insight on several parameters including pore surface coverage by colloids, change of pore void fraction, conductivity and the coordination number between individual colloids in colloid aggregates to show the extent of connection between colloids. As these simulations was designed to not set any of the common assumptions (which neglect the effects of inter-particle forces), the modeling was computationally very expensive. Therefore, in this study, in order to find a practical solution and study any kind of new condition similar to the 162 done cases, a machine learning approach was employed. For training an artificial neural network information 162 simulated cases were used as training feed data. The network consisted of one single hidden layer and

Table 2
Training parameters of network for unfavorable condition.

	Aggregate coordination number	Surface coverage	Conductance	Void fraction
Low ionic strength: *IS* = 0.003				
R	0.9991	0.9998	0.9982	0.9981
MSE	7.4166×10^{-5}	3.1982×10^{-6}	6.3285×10^{-6}	5.1989×10^{-6}
E	6.89	8.88	0.82	0.45
Medium-*IS* = 0.05				
R	0.9998	0.9995	0.9995	0.9989
MSE	7.7409×10^{-5}	6.5990×10^{-6}	2.1806×10^{-5}	4.8983×10^{-6}
E	3.02	3.07	4.6076	1.09
High-*IS* = 0.3				
R	0.9981	0.9988	0.9999	0.9988
MSE	8.0384×10^{-04}	1.7859×10^{-5}	1.7508×10^{-6}	9.1441×10^{-6}
E	6.42	9.28	3.83	1.93

while the transfer function for hidden layer was tangent sigmoid, for the output layer it was chosen to be a pure linear function.

The network architecture had a multi-input and single-output form. This architecture helped to make input–output correlation improved but still it was away from the desired training goal. During the training process, we found that *IS* had a strong nonlinear relationship with the outputs. This strong nonlinearity caused training instability in the model. Therefore, the *IS* was divided to three categories, namely, low, medium, and high *IS*. The training then was conducted individually for three *IS* ranges divided into these three groups.

For adsorption under favorable condition, a maximum relative error of 8.95% was obtained for the training. Correlation coefficients (R) of all ANNs were above 0.995. This R value ensured that network outputs can adequately mimic simulation data in the range of input and output data. In case of adsorption under unfavorable condition, a maximum relative error of 9.3% was obtained, which was sufficient for the training purposes. The correlation coefficients (R) of all ANNs were set above 0.995 by which network outputs would be close enough to simulate data in the range of input and output information. The resulted trained model was able to accurately predict the involved pore properties due to transport of adsorptive through the pore structure.

Finally, it should be noted that, the pore-throat geometry is conveniently but necessarily extremely simplified in this work, and cannot account for naturally occurring discontinuities in surface uniformity or geometry. Therefore, both the flow model, and the arising neural network learning cannot cope precisely with more highly anisotropic systems.

CRediT authorship contribution statement

H. Aslannejad: Conceptualization, Methodology. **H.M. Nezami:** Supervision. **S. Jafari:** Supervision. **A. Raoof:** Supervision.

Declaration of Competing Interest

The authors declare that they have no known competing financial interests or personal relationships that could have appeared to influence the work reported in this paper.

Acknowledgments

We acknowledge prof. J. Foroughi (University of Wollongong) for his support with regard to the training procedure and data preparation. This publication is part of the project PQP (Print Quality and Particles) (with project number 17099) of the research programme Collaboration program High Tech Systemen en Materialen (HTSM) 2018 TTW] which is (partly) financed by the Dutch Research Council (NWO). The first author also acknowledge Deutsche Forschungsgemeinschaft (DFG, German Research Foundation) under Germany's Excellence Strategy-XC2075-390740016.

Appendix A

See Figs. A1-A3.

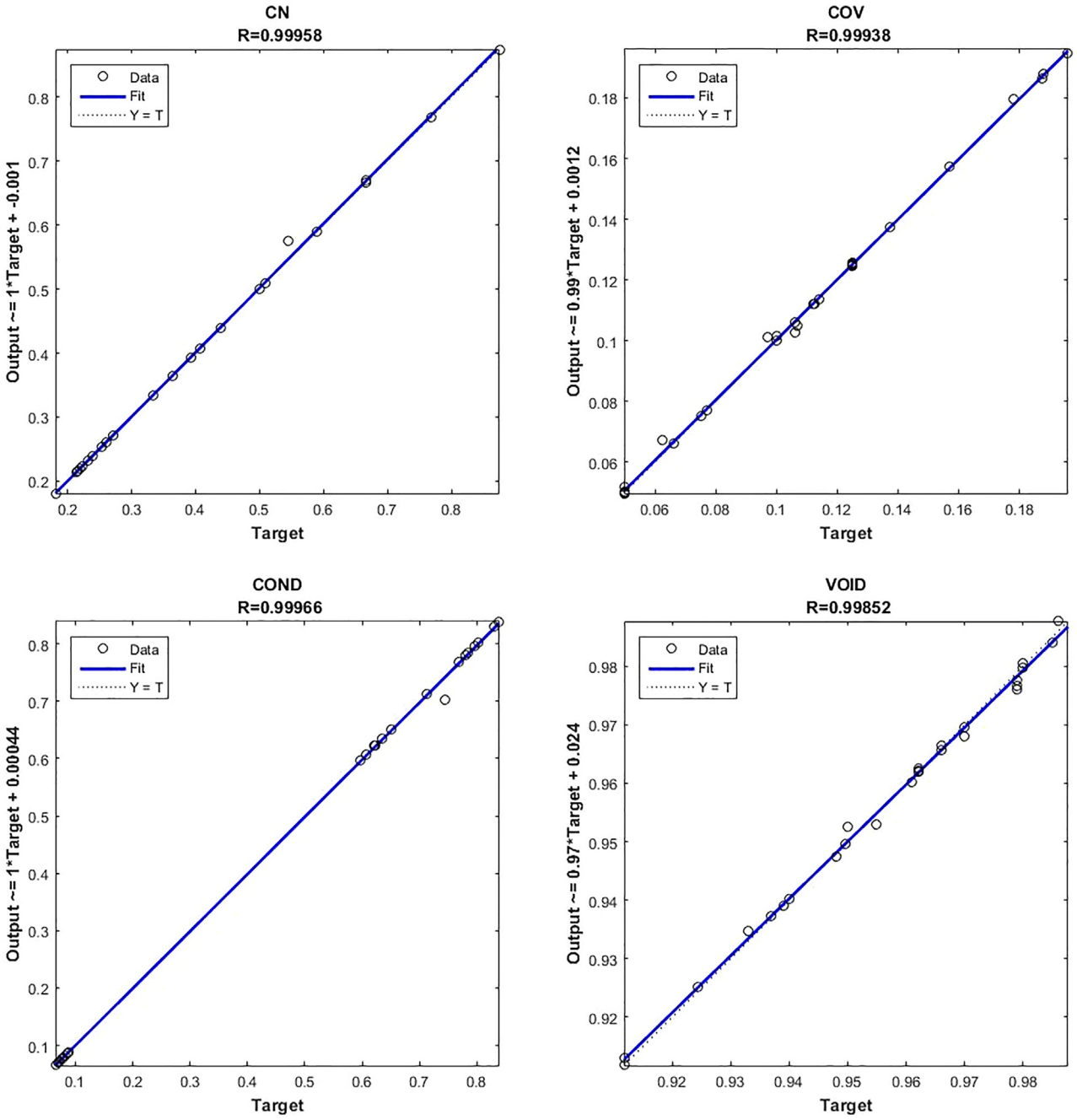

Fig. A1. Regression plots at Low-IS.

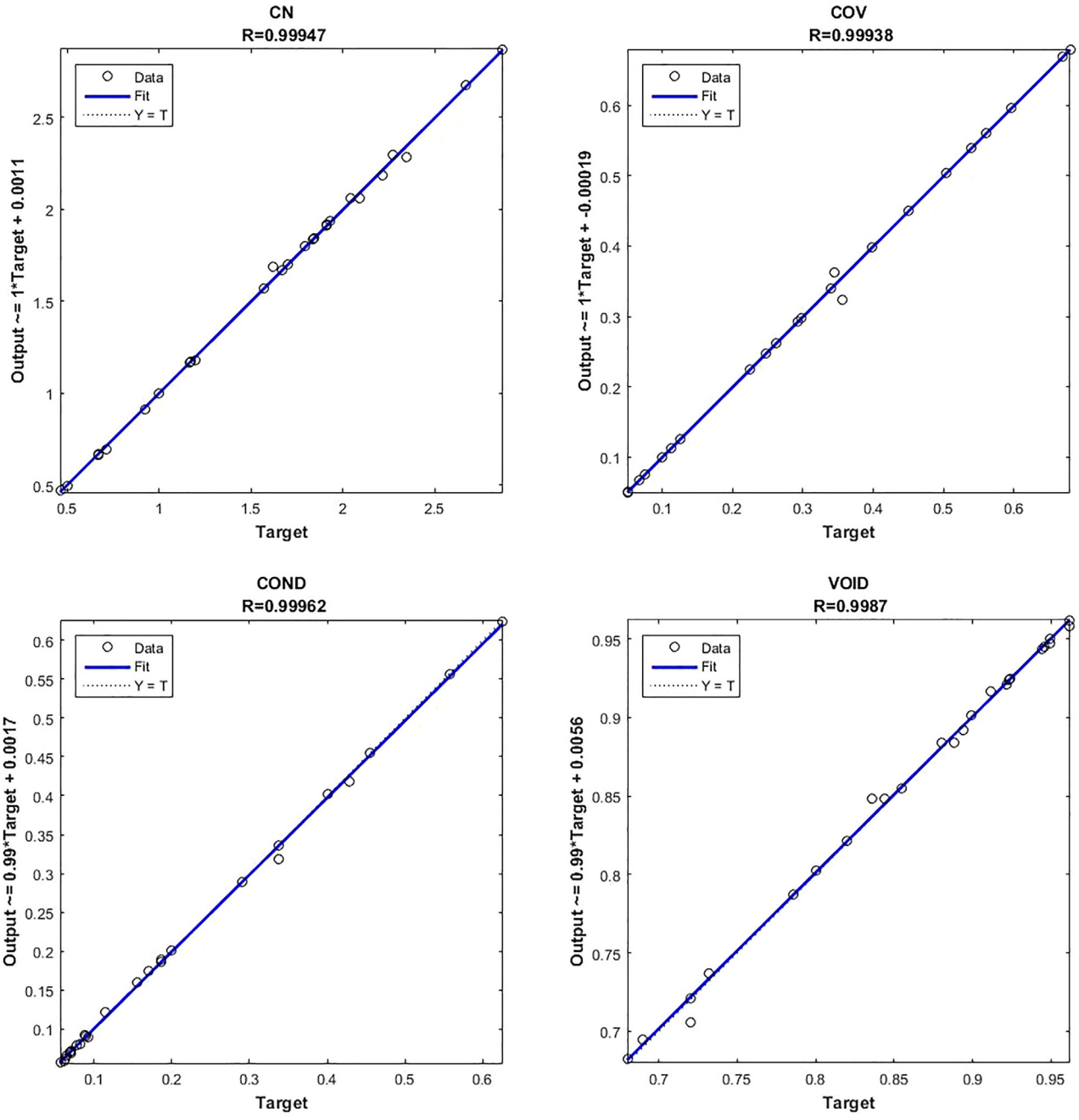

Fig. A2. Regression plots at Medium-IS.

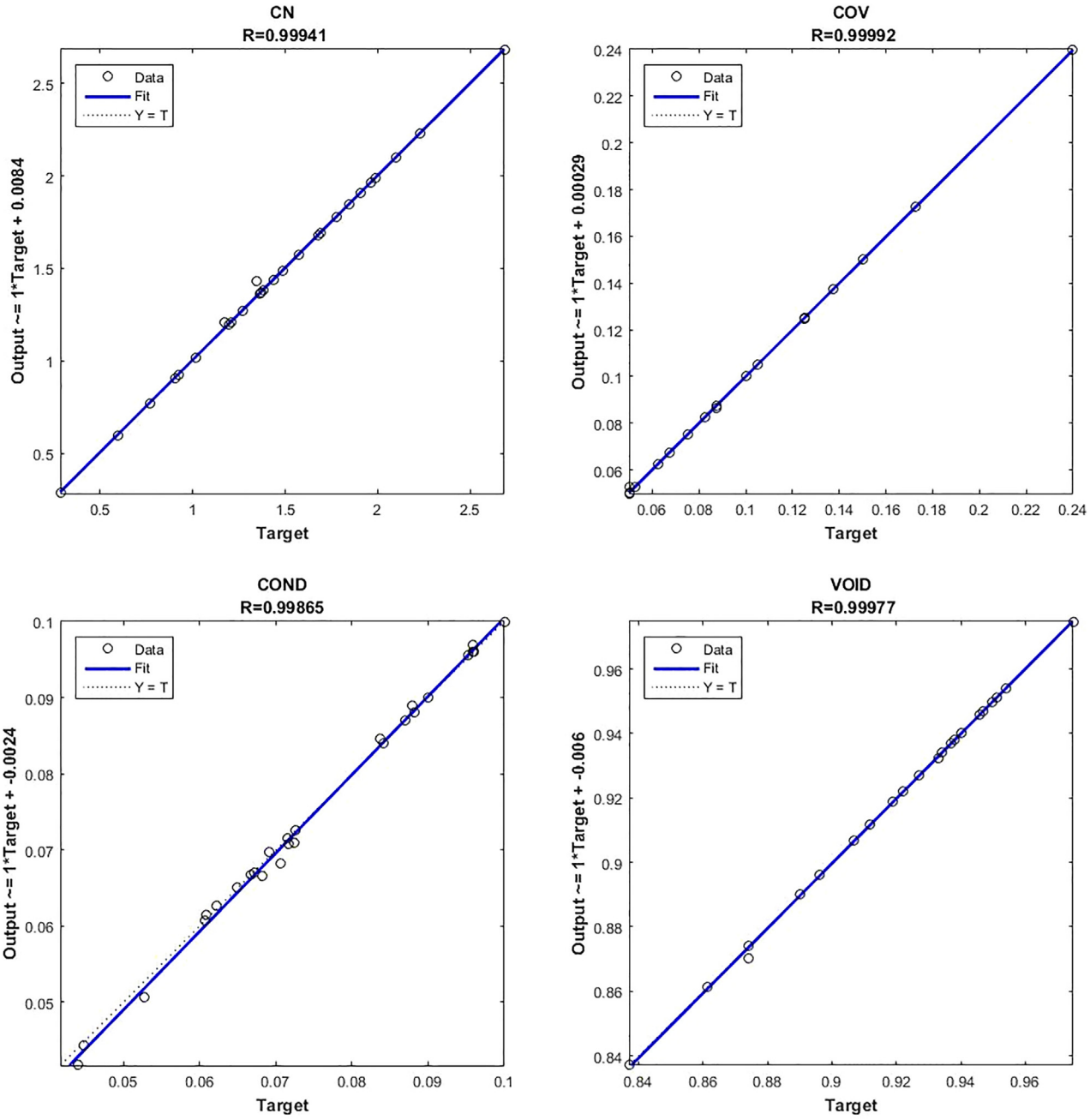

Fig. A3. Regression plots at High-IS.

Appendix B

See Figs. B1-B3.

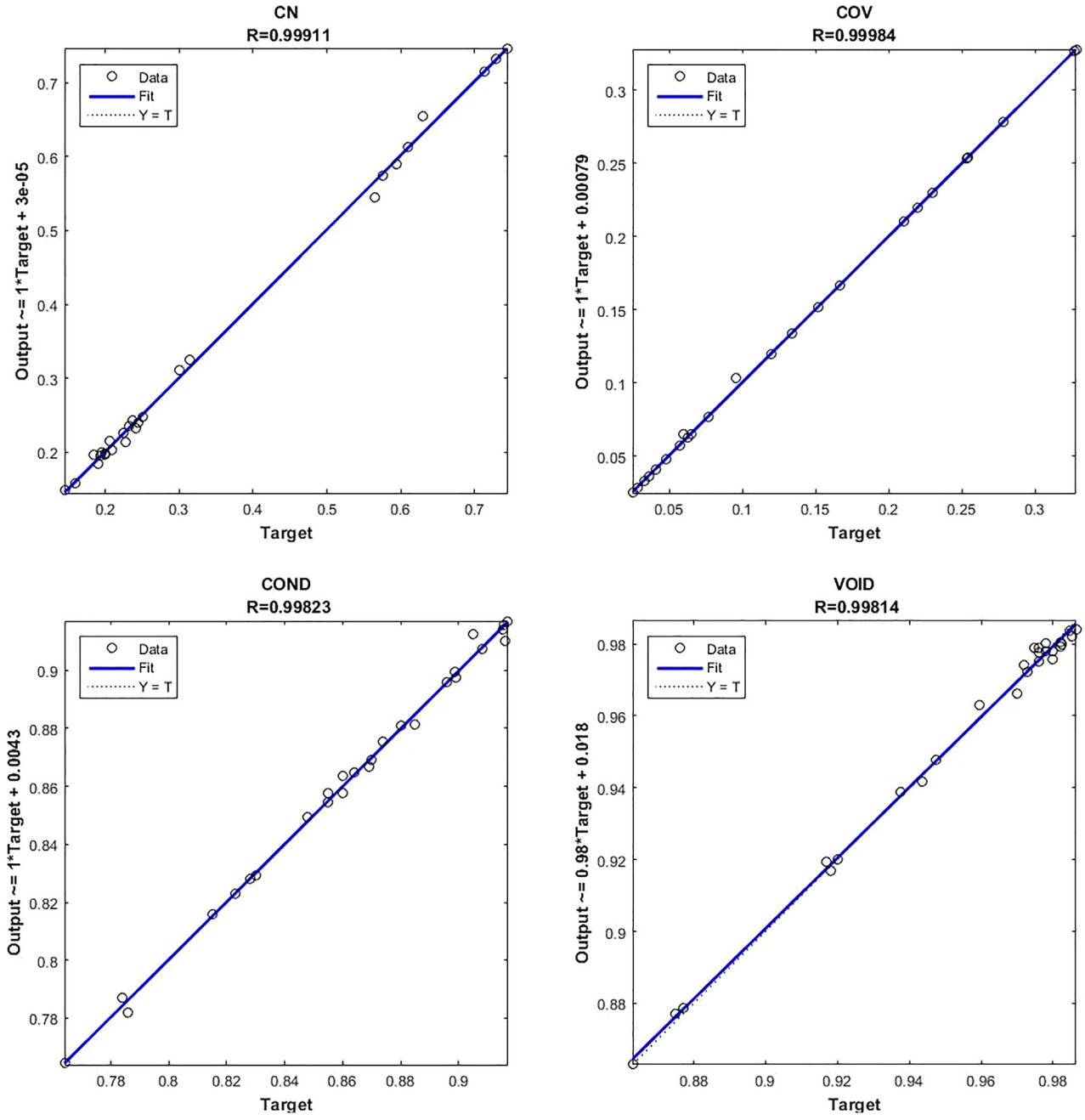

Fig. B1. Regression plots at Low-IS.

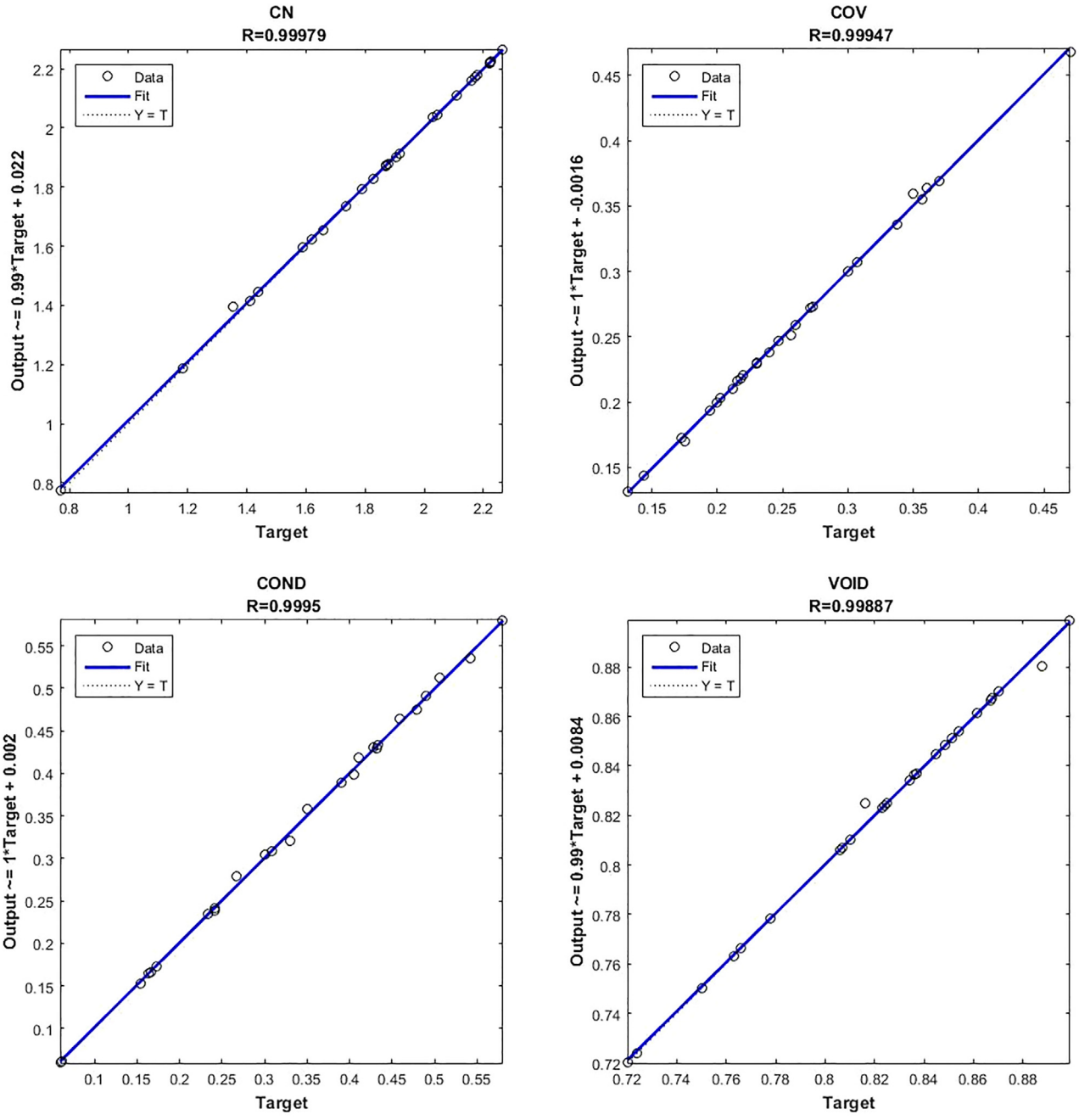

Fig. B2. Regression plots at Medium-IS.

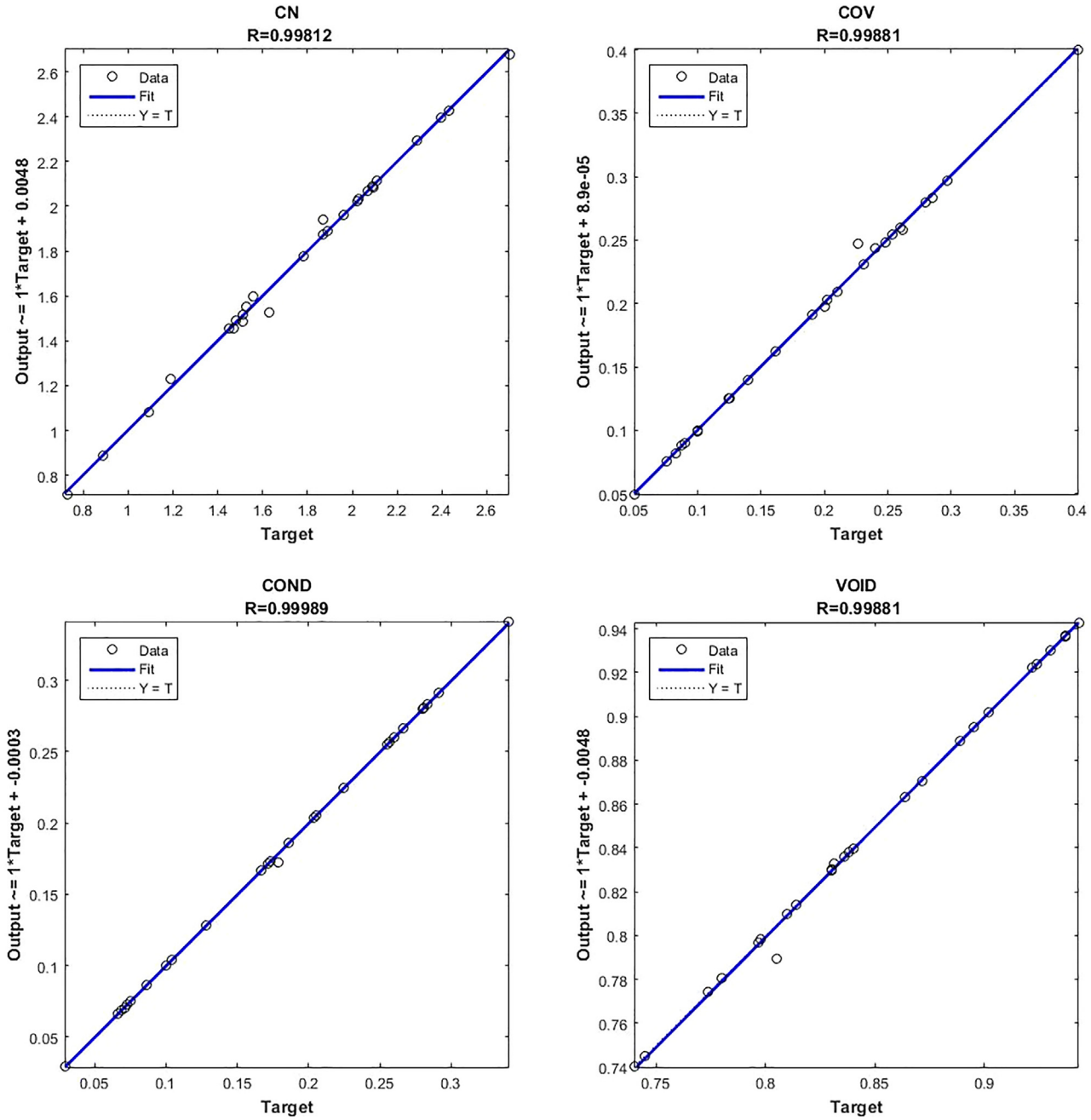

Fig. B3. Regression plots at High-IS.

References

Artificial Neural Network Tutorial - Javatpoint n.d. https://www.javatpoint.com/artificial-neural-network (accessed December 23, 2021).

Aslannejad, H., Hassanizadeh, S.M., Raoof, A., de Winter, D.A.M., Tomozeiu, N., van Genuchten, M.T., 2017. Characterizing the hydraulic properties of paper coating layer using FIB-SEM tomography and 3D pore-scale modeling. Chem. Eng. Sci. 160, 275–280. https://doi.org/10.1016/j.ces.2016.11.021.

Aslannejad, H., Hassanizadeh, S.M., 2017. Study of hydraulic properties of uncoated paper: image analysis and pore-scale modeling. Transp. Porous Media 120 (1), 67–81. https://doi.org/10.1007/s11242-017-0909-x.

Aslannejad, H., Hassanizadeh, S.M., Celia, M.A., 2019. Characterization of the interface between coating and fibrous layers of paper. Transp. Porous Media 127 (1), 143–155. https://doi.org/10.1007/s11242-018-1183-2.

Boek, E.S., Ladva, H.K., Crawshaw, J.P., Padding, J.T., 2008. Deposition of colloidal asphaltene in capillary flow: experiments and mesoscopic simulation†. Energy Fuels 22 (2), 805–813.

Boek, E.S., Wilson, A.D., Padding, J.T., Headen, T.F., Crawshaw, J.P., 2010. Multi-scale simulation and experimental studies of asphaltene aggregation and deposition in capillary flow. Energy Fuels 24 (4), 2361–2368.

Bouzidi, M., Firdaouss, M., Lallemand, P., 2001. Momentum transfer of a Boltzmann-lattice fluid with boundaries. Phys. Fluids 13 (11), 3452–3459. https://doi.org/10.1063/1.1399290.

Bradford, S.A., Simunek, J., Bettahar, M., Van Genuchten, M.T., Yates, S.R., 2006. Significance of straining in colloid deposition: Evidence and implications. Water Resour. Res. 42, 12–15. https://doi.org/10.1029/2005WR004791.

Bradford, S.A., Torkzaban, S., Walker, S.L., 2007. Coupling of physical and chemical mechanisms of colloid straining in saturated porous media. Water Res. 41 (13), 3012–3024. https://doi.org/10.1016/j.watres.2007.03.030.

Buckley, J.S., 2012. Asphaltene deposition. Energy Fuels 26 (7), 4086–4090.

Carvalho, N.B., Minim, V.P.R., Silva R de C dos S.N., Della Lucia, S.M., Minim, L.A., 2013. Artificial neural networks (ANN): prediction of sensory measurements from instrumental data. Food Sci. Technol. 33:722–9

Derjaguin, B., Landau, L., 1993. Theory of the stability of strongly charged lyophobic sols and of the adhesion of strongly charged particles in solutions of

electrolytes. Prog. Surf. Sci. 43 (1-4), 30–59. https://doi.org/10.1016/0079-6816(93)90013-L.

Hu, J., Kim, C., Halasz, P., Kim, J.F., Kim, J., Szekely, G., 2021. Artificial intelligence for performance prediction of organic solvent nanofiltration membranes. J. Memb. Sci. 619, 118513. https://doi.org/10.1016/j.memsci.2020.118513.

Jafari, S., Yamamoto, R., Rahnama, M., 2011. Lattice-Boltzmann method combined with smoothed-profile method for particulate suspensions. Phys. Rev. E - Stat Nonlinear, Soft Matter Phys. 83,. https://doi.org/10.1103/PHYSREVE.83.026702/FIGURES/11/MEDIUM 026702.

Kamrava, S., Tahmasebi, P., Sahimi, M., 2020. Linking morphology of porous media to their macroscopic permeability by deep learning. Transp. Porous Media 131 (2), 427–448. https://doi.org/10.1007/s11242-019-01352-5.

Kamrava, S., Tahmasebi, P., Sahimi, M., 2021. Physics- and image-based prediction of fluid flow and transport in complex porous membranes and materials by deep learning. J. Memb. Sci. 622, 119050. https://doi.org/10.1016/j.memsci.2021.119050.

Krüger, T., Kusumaatmaja, H., Kuzmin, A., Shardt, O., Silva, G., Viggen, E.M., 2017. The Lattice Boltzmann Method. https://doi.org/10.1007/978-3-319-44649-3.

Lattice Boltzmann Method And Its Application In Engineering - Zhaoli Guo, Chang Shu - Google Books n.d. https://books.google.nl/books?hl=en&lr=&id=aDG7CgAAQBAJ&oi=fnd&pg=PR5&dq=Guo+Z,+Shu+C.+Lattice+Boltzmann+method+and+its+application+in+engineering.+World+Scientific%3B+2013+Mar+25&ots=YyL2N_YV8A&sig=FZR-IOTkZLgDH6q_DYuCwivMknA&redir_esc=y#v=onepage&q&f=fa (accessed June 29, 2021).

Lawal, K.A., Vesovic, V., Boek, E.S., 2011. Modeling permeability impairment in porous media due to asphaltene deposition under dynamic conditions. Energy Fuels 25 (12), 5647–5659.

Li, X., Guo, Y., Boek, E.S., Guo, X., 2017. Experimental study on kinetics of asphaltene aggregation in a microcapillary. Energy Fuels 31 (9), 9006–9015.

Samari Kermani, M., Jafari, S., Rahnama, M., Raoof, A., 2020. Direct pore scale numerical simulation of colloid transport and retention. Part I: Fluid flow velocity, colloid size, and pore structure effects. Adv. Water Resour. 144, 103694. https://doi.org/10.1016/j.advwatres.2020.103694.

Samari-Kermani, M., Jafari, S., Rahnama, M., Raoof, A., 2021. Ionic strength and zeta potential effects on colloid transport and retention processes. Colloids Interface Sci. Commun. 42, 100389. https://doi.org/10.1016/j.colcom.2021.100389.

Santos, J.E., Xu, D., Jo, H., Landry, C.J., Prodanović, M., Pyrcz, M.J., 2020. PoreFlow-Net: A 3D convolutional neural network to predict fluid flow through porous media. Adv. Water Resour. 138, 103539. https://doi.org/10.1016/j.advwatres.2020.103539.

Stangierski, J., Weiss, D., Kaczmarek, A., 2019. Multiple regression models and Artificial Neural Network (ANN) as prediction tools of changes in overall quality during the storage of spreadable processed Gouda cheese. Eur. Food Res. Technol. 245 (11), 2539–2547. https://doi.org/10.1007/s00217-019-03369-y.

Sudakov, O., Burnaev, E., Koroteev, D., 2018. Driving digital rock towards machine learning: predicting permeability with gradient boosting and deep neural networks. Comput. Geosci. 127, 91–98. https://doi.org/10.1016/j.cageo.2019.02.002.

Torkzaban, S., Bradford, S.A., van Genuchten, M.T., Walker, S.L., 2008. Colloid transport in unsaturated porous media: The role of water content and ionic strength on particle straining. J. Contam. Hydrol. 96 (1-4), 113–127. https://doi.org/10.1016/j.jconhyd.2007.10.006.

Urang, J.G., Ebong, E.D., Akpan, A.E., Akaerue, E.I., 2020. A new approach for porosity and permeability prediction from well logs using artificial neural network and curve fitting techniques: A case study of Niger Delta, Nigeria. J. Appl. Geophys. 183, 104207. https://doi.org/10.1016/j.jappgeo.2020.104207.

Verwey, E.J.W., 1947. Theory of the stability of lyophobic colloids. J. Phys. Colloid Chem. 51 (3), 631–636.

Wu, J., Yin, X., Xiao, H., 2018. Seeing permeability from images: fast prediction with convolutional neural networks. Sci Bull 63 (18), 1215–1222. https://doi.org/10.1016/j.scib.2018.08.006.

Zou, Q., He, X., 1997. On pressure and velocity boundary conditions for the lattice Boltzmann BGK model. Phys. Fluids 9 (6), 1591–1598. https://doi.org/10.1063/1.869307.